Published in final edited form as:
Eur J Neurosci. 2010 November ; 32(10): 1618–1631. doi:10.1111/j.1460-9568.2010.07447.x.

Polarized Targeting of L1-CAM Regulates Axonal and Dendritic Bundling *in vitro*

Joshua Barry[1], **Yuanzheng Gu**[2], and **Chen Gu**[1,2,*]

[1] Molecular, Cellular, & Developmental Biology Graduate Program, The Ohio State University, Columbus, OH 43210

[2] Department of Neuroscience and Center for Molecular Neurobiology, The Ohio State University, Columbus, OH 43210

Abstract

Proper axonal and dendritic bundling is essential for the establishment of neuronal connections and the synchronization of synaptic inputs, respectively. Cell adhesion molecules of the L1-CAM family regulate axon guidance and fasciculation, neuron migration, dendrite morphology, and synaptic plasticity. How these molecules play so many different roles remains unclear. Here we show that polarized axon-dendrite targeting of an avian L1-CAM protein, NgCAM, can regulate the switch of bundling of the two major compartments of neurons. Using a new *in vitro* model for studying neurite-neurite interactions, we found that expressed axonal NgCAM induced robust axonal bundling via the trans-homophilic interaction of immunoglobulin (Ig) domains. Interestingly, dendritic bundling was induced by the dendritic targeting of NgCAM, caused by either deleting its fibronectin (FN) repeats or blocking activities of protein kinases. Consistent with the NgCAM results, expression of mouse L1CAM also induced axonal bundling and blocking kinase activities disrupted its axonal targeting. Furthermore, the trans-homophilic interaction stabilized the bundle formation, likely through recruiting NgCAM proteins to contact sites and promoting guided axon outgrowth. Taken together, our results suggest that precise localization of L1-CAM is important for establishing proper cell-cell contacts in neural circuits.

Keywords

axon; dendrite; fasciculation; L1-CAM; NgCAM

Introduction

Whereas proper interactions between axons and dendrites are usually required for synapse formation, interactions among axons or among dendrites resulting in axonal or dendritic bundling, respectively, also play critical roles in neural circuitry formation. Selective axonal bundling, or axon fasciculation, is required for the establishment of proper neuronal connections over long distances in nervous systems (Bastiani et al., 1984; Tosney and Landmesser, 1985; Lin et al., 1994; Yu et al., 2000; Hanson et al., 2008). The axon-axon interactions are mediated by cell adhesion molecules (CAMs) and can be regulated by neuronal activity (Walsh and Doherty, 1997; Van Vactor, 1998; Yu et al., 2000; Hanson et al., 2008; Imai et al., 2009). On the other hand, bundling of the apical dendrites of pyramidal

Address correspondence to: Chen Gu, PhD, 182 Rightmire Hall, 1060 Carmack Road, OSU, Columbus, OH 43210. Fax: 614-292-5379; Phone: 614-292-0349; gu.49@osu.edu.

Online supplemental materials include 1 supplemental figure and 6 supplemental movies.

neurons in rat visual cortex (Curtetti et al., 2002), mouse neocortex (Escobar et al., 1986), and somatosensory cortex (Krieger et al., 2007) may regulate electrical coupling and hence the synchronization of synaptic inputs. Dendritic bundles among some retinal neurons may be critical in receiving common excitatory inputs and regulating dendritic fields (He and Masland, 1998; Lohmann and Wong, 2001). A recent study showed that dendritic bundling of gonadotropin-releasing hormone neurons may result in shared synaptic inputs and hence synchronization (Campbell et al., 2009). Moreover, dendritic bundling can be also involved in dendrite-to-dendrite synapse formation, neuron migration, and dendrite morphogenesis during development. Compared to axonal bundling, much less is known regarding how dendritic bundling is established and regulated. Regulation of axonal and dendritic bundling by the same CAM is an intriguing possibility.

Members of the L1-CAM family, including L1, CHL1 (close homolog of L1), Neurofascin, and NrCAM, play pivotal roles in axon outgrowth, guidance and fasciculation, neuronal migration and survival, and synaptic plasticity. These molecules contain six immunoglobulin-like (Ig) domains and four to five fibronectin type III (FN) repeats in the extracellular region. They also contain a single membrane-spanning segment, followed by a highly conserved cytoplasmic tail in the C-terminus. The adhesive function of L1-CAM between neurons is mediated by both heterophilic and homophilic interactions via the Ig domains (Maness and Schachner, 2007). The intracellular trafficking of L1-CAM is usually mediated by the cytoplasmic C-terminus, in which a conserved sequence (FIGQ/AY) binds to ankyrin proteins, critical adaptor proteins linking L1 to the actin cytoskeleton (Bennett and Chen, 2001). Moreover, L1 C-terminus also binds ezrin-radixin-moesin proteins (Dahlin-Huppe et al., 1997; Dickson et al., 2002). Mutations in human L1 gene are responsible for a wide spectrum of neurological abnormalities, including corpus callosum hypoplasia, aphasia, adducted thumbs, spastic paraplegia, optic nerve atrophy and hydrocephalus, and mental retardation (Fransen et al., 1997; De Angelis et al., 2002; Maness and Schachner, 2007). Knockout mice carrying mutations of L1-CAM showed not only abnormalities of corticospinal, retino-collicular, thalamocortical, and callosal axons (Cohen et al., 1998; Demyanenko and Maness, 2003; Wiencken-Barger et al., 2004), but also abnormal dendritic bundles of cortical pyramidal neurons (Dahme et al., 1997; Demyanenko et al., 2004; Maness and Schachner, 2007). How L1-CAM proteins are involved in both axon and dendrite morphogenesis is unclear.

Different L1-CAM proteins display distinct expression and targeting patterns, which may result in their different roles in axon and dendrite morphogenesis. NgCAM is the chicken homolog of L1. Expressed NgCAM is used as a model molecule to understand basic molecular mechanisms underlying polarized membrane protein sorting and targeting of hippocampal neurons (Wisco et al., 2003; Sampo et al., 2003; Yap et al., 2008a; Yap et al., 2008b). In this study, we have developed a new *in vitro* system to test our hypothesis that axonal and dendritic bundling can be regulated by the axon-dendrite targeting of a single L1-CAM protein. By using a modified transfection method, we were able to express different constructs into different neurons in the same culture and to study the interactions among their neurites. We found that axonal NgCAM induced robust axonal bundling through the binding of their extracellular Ig domains. Remarkably, the axonal bundling was switched to dendritic bundling by reversing the polarized targeting of NgCAM by either mutagenesis or blocking protein kinase activities. Therefore, our data suggest that the axon-dendrite targeting of L1-CAM is critical for establishing proper subcellular contacts in neural circuit formation.

Materials and Methods

cDNA constructs and antibodies

NgCAM-GFP is a kind gift from Dr. Gary Banker. In this construct, the stop codon of NgCAM is eliminated. In the linker region between NgCAM and GFP, there is an EcoRI site. There is another EcoRI site after the GFP region. Thus, the GFP coding region can be easily cut out by an EcoRI digestion. NgCAM-mCherry was constructed by inserting the cDNA fragment PCRed from the mCherry (a kind gift from Dr. Roger Tsien) coding region into the EcoRI sites. The construct with mCherry in the right orientation has red fluorescence when expressed in neurons. NgCAM-ΔIg-GFP and NgCAM-ΔIg-mCh (mCherry) were constructed by deleting the Ig domains between residues Q35 and F539, where two XhoI sites in the same reading frame were engineered by Quickchange. Two rounds of the Quickchange mutagenesis were used to generate the NgCAM construct with two engineered XhoI sites. The construct was cut with XhoI and religated without the insert. Using the same strategy, NgCAM-ΔFN-GFP and NgCAM-ΔFN-mCh were made by deleting the fibronectin repeat domain between residues I609 and F1140. NgCAM-ΔCt-GFP and NgCAM-ΔCt-mCh were made by deleting the intracellular C-terminal region between Y1174 and D1280. ICAM5-GFP and mL1CAM-GFP were made by inserting the coding sequences PCRed from ICAM5 and mouse L1CAM (OpenBiosystem, Huntsville, AL, USA) into the pEGFP-N1 vector (Clontech, Maintain View, CA, USA), respectively. All the constructs were confirmed with sequencing.

The following antibodies were used: rabbit polyclonal anti-MAP2 (Chemicon, Temecula, CA, USA), rabbit polyclonal anti-Tau1 (Abcam, Cambridge, MA, USA), mouse monoclonal anti-NgCAM antibody (8D9, Developmental Studies Hybridoma Bank, Iowa City, IA, USA), mouse monoclonal anti-GFP antibody (Antibodies Inc., Davis, CA, USA), Cy5-conjugated secondary antibody (Jackson ImmunoResearch, West Grove, PA, USA).

Hippocampal neuron culture and transfection

Primary dissociated hippocampal neuron culture was prepared from pregnant Sprague-Dawley rats at embryonic day 18 (E18) under sterile conditions as previously described (Gu et al., 2006; Xu et al., 2007), in accordance with ethical guidelines stipulated by the animal ethics committee, the Ohio State University. The rats were killed by CO_2 exposure. Hippocampi were dissected from E18 rat embryos. Embryonic hippocampal neurons were disassociated in the dissecting medium (in mM, 82 Na_2SO_4, 30 K_2SO_4, 10 HEPES (pH 7.4), 10 glucose, 6 $MgCl_2$, and 3 mg/ml Protease 23 (Sigma, St. Louis, MO, USA)), resuspended in the plating medium (MEM Earle's salts, 1 mM sodium pyruvate, 25 μM L-Glutamine, 0.45% glucose, 10% FBS, and 1X Pen/Step (Invitrogen, Carlsbad, CA, USA)), and plated onto glass coverslips coated with poly-D-Lysine (Sigma) and collagen (Roche, Mannheim, Germany). Two to fours hrs after plating, when neurons attached to coverslips, the plating medium was replaced by the maintenance medium (Neurobasal medium, 1X B27 supplement (Invitrogen), 0.5 mM L-Glutamine, and 1X Pen/Strep). Two days after neuron plating, 1 μM cytosine arabinose (Sigma) was added to the maintenance medium to inhibit glial growth for the subsequent 2 days, then replaced with the normal maintenance medium. The maintenance medium was replenished twice a week by replacing a half volume.

The transfection procedure was modified for studying neuron interactions. Cultured neurons at 5 DIV (day *in vitro*) were incubated in Opti-MEM containing 0.4 μg cDNA plasmid of the first construct mixed with 0.75 μl Lipofectamine 2000 (Invitrogen) and 0.4 μg cDNA plasmid of second construct mixed with 0.75 μl Lipofectamine 2000 for 20 min at 37°C. Thus, each cDNA/cationic lipid complex contained only one type of cDNA plasmid so that

each neuron likely expressed only one protein construct. With this transfection method, over 95% of transfected neurons expressed only one construct.

Drug treatment

The following chemicals were used. Chelerythrine chloride (a PKC inhibitor), p38 MAP kinase inhibitor III, staurosporine (a broad-spectrum Ser/Thr kinase inhibitor), JNK inhibitor II, KT5823 (a PKG inhibitor), Rp-cAMPS (a PKA inhibitor), ML-7 hydrochloride (a myosin light chain kinase inhibitor), KN-93 (a selective Ca^{2+}/calmodulin-dependent protein kinase II inhibitor), PD98059 (a MEK1 inhibitor), genistein (a tyrosine kinase inhibitor), GSK inhibitor IX, and U0126 (a MEK1/2 inhibitor) were purchased from Calbiochem (Gibbstown, NJ, USA). 4-aminopyridine (4-AP), tetrodotoxin (TTX), ethanol, and carbachol chloride were purchased from Sigma.

Drugs were added 4–6 hours after transfection in proper concentration. Neurons were usually treated for 48 hrs before fixation and staining. Within this time window and under the drug concentration used, no detrimental effect on neuron survival was observed.

Immunofluorescence staining

The procedure of immunocytochemistry and fluorescence microscopy was described previously (Gu et al., 2006; Xu et al., 2007). In brief, the neurons expressing NgCAM or mL1CAM constructs were fixed and stained under permeabilized conditions (in the presence of 0.2% Triton) for endogenous dendritic marker microtubule associated protein 2 (MAP2) or axonal marker Tau1. To reveal the surface level of NgCAM constructs, the transfected neurons were first stained with the 8D9 antibody under non-permeabilized conditions, permeabilized with 0.2% Triton after washing, and then stained with the anti-MAP2 antibody.

Fluorescence imaging and quantification

Fluorescence images were captured with a Spot CCD camera RT slider (Diagnostic Instruments, Sterling Heights, MI, USA) mounted on a Zeiss (Oberkochen, Germany) upright microscope, Axiophot, using Plan Apo objectives 20 ×/0.75 and 100 ×/1.4 oil, saved as 16-bit TIFF files, and analyzed with NIH ImageJ and Sigmaplot 10.0 for fluorescence intensity quantification. Exposure times were controlled so that the pixel intensities in dendrites and axons were below saturation, but the same exposure time was used within each group of an experiment. The quantification procedure for axon-dendrite targeting ratio ($F_{\boldsymbol{axon}}/F_{\boldsymbol{dendrite}}$) was described previously (Gu et al., 2006; Xu et al., 2007). Only transfected neurons with clearly separated dendrites and axons, and isolated from other transfected neurons were chosen for analysis. The co-staining with axonal marker Tau1 and/or dendritic marker MAP2 helped to distinguish axons from dendrites. We determined the targeting ratio ($F_{\boldsymbol{axon}}/F_{\boldsymbol{dendrite}}$), the average fluorescence intensity in axons divided by the average fluorescence intensity in dendrites. To measure the fluorescence intensity, we laid lines along the major processes to acquire the fluorescence intensity profiles (in arbitrary unit) of these processes excluding segments fasciculated with other neurites, regions with crossings, proximal dendritic segments within 20 μm from the soma, and fine terminal branches.

Here is the procedure for the quantification of the axonal bundling index (ABI). Measurements of the RGB image of a pair of neurons with green and red fluorescence were performed with NIH Image J. The total length of bundled axonal segments between a green and red neuron (L_{total} in μm) was measured. The number of crossings between the green and red axons (N_{cross}) was manually counted. Each bundled segment was counted as one crossing. The ABI for this pair of neurons was defined as the average length of bundled axons per crossing (ABI in μm/crossing), ABI = L_{total}/N_{cross}. Thus, we obtained the ABI for

each pair of neurons. An example is provided in Fig. 2C. For each condition, more than 10 pairs of neurons from at least three independent transfections were quantified and their ABIs are given with means and standard errors.

Fluorescence recovery after photobleaching (FRAP) imaging

To better visualize the moving carriers containing NgCAM-GFP, we adopted the strategy of FRAP imaging. First, the GFP fluorescence of NgCAM-GFP in an axonal segment (50 ~150 μm) was bleached by maximal excitation lights for 5 to 10 min. Then we performed time-lapse imaging using weaker excitation lights (~12.5% of the maximal) with the 8× neutral density filter to visualize NgCAM-GFP-containing carriers moving from the unbleached regions through the bleached segment. For instance, in isolated axons we frequently observed anterograde axonal transport of NgCAM-GFP-containing carriers (Fig. 7A; movie 1). The velocity for individual moving carrier was calculated by dividing the travel distance with the time.

Two-color time-lapse imaging

Neurons growing on 25 mm coverslips were loaded into the imaging chamber (Molecular Devices, Downingtown, PA, USA) and incubated with the long-term imaging buffer (HE-LF medium (Brainbits, Springfield, IL, USA) plus 2% B-27, 0.5 mM Glutamine, and 25 μM Glutamate) at room temperature. The time-lapse imaging setup was built upon a Nikon (Nikon Inc., Melville, NY, USA) TE2000 inverted microscope. Images were captured with a CCD camera Coolsnap HQ (Photometrics, Tucson, AZ, USA) through FITC (for GFP) and TexRd (for mCherry) filters with 2 sec exposure time. The filters were changed through filter wheels controlled through Lamda 10-3 (Sutter Instrument, Novato, CA, USA) by the MetaMorph software (Molecular Devices). The time-lapse was performed with a 5 min interval for 150 frames.

Statistical analysis

All data were analyzed with PASW/SPSS Statistics 18 (SPSS Inc., Chicago, IL, USA) and are presented as the mean ± SEM. Two-tailed Student's *t*-test was used for comparisons between two groups. One-way ANOVA followed by Dunnett's test was used for comparing three or more groups. $P < 0.05$ was considered statistically significant.

Results

NgCAM expression induces robust axonal bundling in cultured hippocampal neurons

To study neurite-neurite interactions mediated by L1-CAM, we developed a new method to express GFP- and mCherry-tagged proteins in different neurons in culture. We modified the transfection procedure of Lipofectamine 2000 to ensure each cDNA/cationic lipid complex contained only one type of cDNA plasmid. Transfecting neurons with two such complexes resulted in one protein expressed in one neuron (see Materials and Methods). GFP or mCherry was fused to the cytoplasmic C-terminus of NgCAM, a chicken homolog of L1. Cultured hippocampal neurons were transfected at 5 DIV and fixed 3 days later. The axons of NgCAM-GFP- and NgCAM-mCherry-expressing neurons became extensively bundled (Fig. 1A). The length of bundled axons gradually increased as the transfected neurons grew older. As a negative control, soluble GFP and mCherry were transfected into neurons using the same strategy described above. Indeed almost no axonal bundling was observed between the axons of GFP- and mCherry-expressing neurons, despite their extensive crossings (Fig. 1B).

By using soma and axonal growth cones to determine the orientation of the axons, we identified a variety of axonal bundles and categorized them into three major groups. In the

first group, two axonal growth cones highly colocalized (Fig. 1C), suggesting that they may interact and migrate together. The trailing growth cone was relatively smaller than the leading one (Fig. 1C). In the second group, an axonal growth cone was migrating along an axon in the same (Fig. 1D) or opposite direction (Fig. 1E). The growth cones of the trailing axons were very small (Fig. 1D,E), which is consistent with the previous observation in zebrafish commissural fascicles (Bak and Fraser, 2003). In the third group, bundled axons differed in diameter and formed branches (Fig. 1F,G). These interesting patterns of bundled axons prompted us to pursue the underlying mechanism.

Different roles of NgCAM domains in axonal bundling

Deleting the extracellular Ig domains completely eliminated axonal bundling induced by expressed NgCAM constructs (Fig. 2A). Despite extensive crossings between the NgCAM-ΔIg-GFP- and NgCAM-ΔIg-mCh-expressing axons, almost no axonal bundling was observed (Fig. 2A). Moreover, compared to the wildtype NgCAM, deletion of its Ig domains significantly increased axonal branching (Fig. 2A). Thus, the results obtained with the new system show that the Ig domains essential for the trans-homphilic interaction were indeed required in axonal bundling. Interestingly, deleting the intracellular C terminus reduced axonal bundling (Fig. 2B). The localization pattern of NgCAM-ΔCt-GFP along axons was largely similar to that of NgCAM-GFP, except that the C-terminal deletion formed more punctuate clusters along axons.

To quantify the degree of axonal bundling affected by various domains of NgCAM, we measured axonal bundling after transfection of deletion constructs of NgCAM-GFP and NgCAM-mCherry. Pairs of green and red neurons with at least one axonal contact were selected for quantification. The total length of bundled axonal segments and the total number of axonal crossings between green and red neurons were then measured (Fig. 2C). The axonal bundling index (ABI) was defined as the total length of bundled axonal segments divided by the total number of crossings.

The ABIs reflected the significant difference in the degree of axonal bundling between a pair of NgCAM-GFP- and NgCAM-mCherry-expressing neurons (NgCAM-GFP and NgCAM-mCherry ABI: 107.88 ± 9.26 μm/crossing; n = 30; One-way ANOVA, $F_{4, 155}$ = 66.893, $P < 0.001$) and a pair of GFP-and mCherry-expressing neurons as control (GFP and mCherry ABI: 2.86 ± 0.78 μm/crossing; n = 32) (Fig. 2D). Almost no axonal bundling was induced by the expression of NgCAM Ig domain deletions (NgCAM-ΔIg-GFP and NgCAM-ΔIg-mCh ABI: 1.12 ± 0.56 μm/crossing; n = 20; One-way ANOVA, $F_{4, 155}$ = 66.893, $P < 0.999$), similar to the negative control (Fig. 2D). The axonal bundling induced by the C-terminal deletion significantly decreased (NgCAM-ΔCt-GFP and NgCAM-ΔCt-mCh ABI: 61.45 ± 6.62 μm/crossing; n = 35; One-way ANOVA, $F_{4, 155}$ = 66.893, $P < 0.001$), compared to the wild type NgCAM (Fig. 2D). The axonal bundling induced by the extracellular FN domain deletions was only slightly more (NgCAM-ΔFN-GFP and NgCAM-ΔFN-mCh ABI: 18.30± 2.88μm/crossing; n = 43; One-way ANOVA, $F_{4, 155}$ = 66.893, $P = 0.103$) compared to the control, but the difference was not statistically significant (Fig. 2D). Compared to the wild type NgCAM, the ABIs of all three truncations markedly decreased (One-way ANOVA, $F_{3, 124} = 56.366$, $P < 0.001$) (Fig. 2D).

Axons of the neurons expressing NgCAM constructs were confirmed with axonal marker Tau1 (Fig. S1). Bundled axons from the neurons expressing NgCAM-GFP and NgCAM-mCherry or from the neurons expressing NgCAM-ΔCt-GFP and NgCAM-ΔCt-mCh were clearly Tau1-positive (Fig. S1A,C). Unbundled axons from the neurons expressing either Ig- or FN-deletion of NgCAM constructs were also Tau1-positive (Fig. S1B,D). However, it is important to note that at 8 DIV Tau1 staining tends to concentrate in distal axons and thus not every axonal segment has the exact same intensity of Tau1 staining. Moreover, Tau1

staining signals in somatodendritic regions were from the axons traveling along dendrites and neuronal soma. Nonetheless, the axonal and dendritic targeting of NgCAM constructs was clearly determined in this study.

Dendritic bundling induced by the dendritic targeting of NgCAM constructs

Surprisingly, expression of the FN deletion constructs induced a significant amount of dendritic bundling (Fig. 3A–C). The dendritic bundles displayed multiple modes. The dendrites from two different neurons grew along each other in the opposite (Fig. 3A,B) or same direction (Fig. 3A,C). Axonal and dendritic bundling could form simultaneously within a pair of neurons (Fig. 3C). The bundled dendrites in both the same and reverse orientation were confirmed with the staining of dendritic marker, MAP2 (microtubule-associated protein 2) (Fig. 3A). Therefore, the NgCAM constructs lacking the FN domain induced dendritic bundling, which was not normally observed with wildtype constructs. However, targeting an Ig-domain-containing CAM onto dendritic membranes was not sufficient to induce dendritic bundling. Expression of the constructs of dendritic ICAM5 (intercellular adhesion molecule 5, telencephalin), which mediates cell-cell interactions via the homophilic binding between extracellular Ig domains, did not induce dendritic bundling (Fig. 3D), even though the extracellular domain of ICAM5 contains nine Ig domains. Consistent with the data using Tau1 co-staining (Fig. S1), NgCAM wild type, andΔCt andΔIg constructs were highly enriched in axons that were MAP2-negative (Fig. 3E), in contrast to the somatodendritic localization of NgCAM-ΔFN (Fig. 3A–C). Therefore, we hypothesized that the axonal and dendritic bundling was determined by the polarized axon-dendrite targeting of NgCAM.

Next, we examined the targeting patterns on neuronal membranes using an anti-NgCAM (8D9, against the extracellular Ig domains) antibody under non-permeabilized conditions. NgCAM-GFP was highly enriched on axonal membranes (Fig. 4A,D,F; $F_{axon}/F_{dendrite}$: 6.72 ± 0.70; n = 17), consistent with previous studies (Sampo et al., 2003; Wisco et al., 2003). Deleting the entire C-terminal domain did not alter the polarity of axonal targeting—NgCAM-ΔCt-GFP was still enriched on axonal membranes (Fig. 4B,D,F; $F_{axon}/F_{dendrite}$: 5.71 ± 0.74; n = 15; One-way ANOVA, $F_{2, 42} = 28.723$, $P = 0.404$; Compared to NgCAM-GFP). In contrast, deleting the FN domain reversed the polarity of NgCAM targeting. NgCAM-ΔFN-GFP became highly enriched on dendritic membranes (Fig. 4C,D,F; $F_{axon}/F_{dendrite}$: 0.28 ± 0.03; n = 13; One-way ANOVA, $F_{2, 42} = 28.723$, $P < 0.001$; Compared to NgCAM-GFP). We also examined another control, ICAM5-GFP and found that its GFP fluorescence reflecting the total protein was mainly concentrated in dendrites (Fig. 4F; $F_{axon}/F_{dendrite}$: 0.35 ± 0.04; n = 12). All the GFP fusion constructs were expressed in the right size (Fig. 4E). Therefore, this correlation of axon/dendrite bundling and targeting suggest that polarized membrane targeting of NgCAM regulates the formation of axonal and dendritic bundling.

Protein phosphorylation regulates NgCAM targeting and hence neurite bundling

To identify the signaling pathway involved in regulating axonal and dendritic bundling, we treated the neurons expressing NgCAM-GFP or NgCAM-mCherry with drugs aimed at different targets. The ABI for each treatment was calculated and compared to the untreated (ABI: 102.3 ± 8.2μm/crossing; n = 15). First, we examined whether the activities of voltage-gated ion channels affected the NgCAM- induced axonal bundling, since neuronal firing patterns were shown to regulate axon fasciculation (Hanson and Landmesser, 2004, 2006). The treatments with 2 μM tetrodotoxin (TTX; ABI: 104.4 ± 8.3μm/crossing; n = 11; One-way ANOVA, $F_{3, 47} = 1.885$, $P = 0.998$) to block voltage-gated sodium (Nav) channels, 100 μM 4-aminopyridine (4-AP; ABI: 121.5 ± 15.5μm/crossing; n = 10; One-way ANOVA, $F_{3, 47} = 1.885$, $P = 0.179$) to block voltage-gated potassium (Kv) channels, or 50 nM Cd^{2+}

(ABI: 95.0 ± 11.5μm/crossing; n = 15; One-way ANOVA, $F_{3, 47} = 1.885$, $P = 0.924$) to block voltage-gated calcium (Cav) channels, did not significantly affect NgCAM-induced axonal bundling (Fig. 5E). Therefore, changing neuronal excitability might not generate the right action potential firing pattern to regulate neurite bundling.

Next, we examined the effect of carbachol, an agonist of acetylcholine receptors. The carbachol treatment significantly enhanced the axonal bundling (ABI: 136.0 ± 7.5μm/crossing; n = 13; Two-tailed Student's *t*-test, $t_{26} = -2.708$, $P = 0.011$) (Fig. 5A,E). Carbachol activates both ligand-gated nicotinic and G protein-coupled muscarinic receptors. Whereas the activation of nicotinic receptors increases neuronal excitability, the activation of muscarinic receptors initiates various protein kinase pathways through G proteins and thereby may change neuronal firing patterns. Therefore, we examined the effects of several protein kinase inhibitors. Chelerythrine (Chele) (an inhibitor of protein kinase C (PKC); ABI: 86.2 ± 12.1μm/crossing; n = 11; One-way ANOVA, $F_{8, 86} = 2.820$, $P = 0.935$), Rp-cAMPS (an inhibitor of protein kinase A (PKA); ABI: 96.0 ± 10.8μm/crossing; n = 12; One-way ANOVA, $F_{8, 86} = 2.820$, $P = 1.000$), KN-93 (an inhibitor of Ca^{2+}/calmodulin dependent kinase (CAMK); ABI: 86.9 ± 15.1 μm/crossing; n = 10; One-way ANOVA, $F_{8, 86} = 2.820$, $P = 0.916$), ML-7 (an inhibitor of myosin light chain kinase (MLCK); ABI: 127.4 ± 14.3 μm/crossing; n = 10; One-way ANOVA, $F_{8, 86} = 2.820$, $P = 0.649$), KT5823 (an inhibitor of protein kinase G (PKG); ABI: 100.4 ± 10.7 μm/crossing; n = 11; One-way ANOVA, $F_{8, 86} = 2.820$, $P = 1.000$), GSK3 inhibitor (ABI: 115.2 ± 2.4 μm/crossing; n = 10; One-way ANOVA, $F_{8, 86} = 2.820$, $P = 0.984$), and genistein (an inhibitor of tyrosine kinases; ABI: 84.0 ± 10.9μm/crossing; n = 10; One-way ANOVA, $F_{8, 86} = 2.820$, $P = 0.894$), had no major effect on the NgCAM-induced axonal bundling (Fig. 5E). In contrast, staurosporine (Stau; ABI: 32.8 ± 2.26μm/crossing; n = 6; One-way ANOVA, $F_{8, 86} = 2.820$, $P = 0.009$), a broad-spectrum protein kinase inhibitor, substantially decreased axonal bundling and induced dendritic bundling (Fig. 5B,E). To determine how the Stau treatment resulted in a switch from axonal to dendritic bundling, we examined the membrane targeting of NgCAM-GFP. Remarkably, the polarity of axon-dendrite targeting of NgCAM-GFP was reversed by the Stau treatment (Fig. 5C). Therefore, these pharmacological results support our hypothesis based on mutagenesis studies that polarized axon-dendrite targeting of L1-CAM regulates axonal and dendritic bundling.

To identify the kinase(s) potentially involved in regulating polarized targeting of NgCAM and NgCAM-induced neurite bundling, we further examined the effects of specific inhibitors blocking three different pathways of mitogen-activated protein (MAP) kinases. Only the inhibition of c-Jun N-terminal kinases (JNKs) by JNK inh (ABI: 68.7 ± 10.3 μm/crossing; n = 11; One-way ANOVA, $F_{4, 43} = 2.370$, $P = 0.018$), significantly reduced axonal bundling induced by the expression of NgCAM constructs (Fig. 5D,E). Inhibition of either extracellular signal-regulated kinases (ERKs) by PD98059 (ABI: 83.2 ± 6.3 μm/crossing; n = 12; One-way ANOVA, $F_{4, 43} = 2.370$, $P = 0.353$) or by U0126 (ABI: 96.5 ± 13.6 μm/crossing; n = 11; One-way ANOVA, $F_{4, 43} = 2.370$, $P = 0.753$), or p38 MAP kinases by p38 inh (ABI: 80.4 ± 6.4 μm/crossing; n = 11; One-way ANOVA, $F_{4, 43} = 2.370$, $P = 0.215$), had no effect on the induced axonal bundling (Fig. 5E).

Previous studies showed that over-expression does not disrupt the axonal targeting of NgCAM or L1 (Sampo et al., 2003; Wisco et al., 2003; Dequidt et al., 2007). The endogenous L1 level is low in cultured rat hippocampal neurons. It was estimated that over-expressed L1-GFP was approximately five fold higher than the endogenous L1 (Dequidt et al., 2007). To assess whether our findings with NgCAM are applicable to the L1-CAM, we fused a GFP to the mouse L1CAM (mL1CAM, almost identical to the rat L1) C-terminus and examined its targeting and its effect on neurite bundling. Consistent with the results of NgCAM-GFP, mL1CAM-GFP was mainly targeted to axons (Fig. 6A,C) and its polarized

axon-dendrite targeting was also reversed by the Stau treatment (Fig. 6B,C). Interestingly, mL1CAM-GFP-expressing neurons formed extensive axonal bundles with the NgCAM-mCherry-expressing neurons (Fig. 6D), suggesting that they can bind to each other *in trans* presumably through their extracellular Ig domains. Taken together, our findings suggest that our data with NgCAM can represent the targeting and bundling of rodent L1CAM.

Axonal transport and neurite movements in bundle formation stabilized by the trans-homophilic interaction of NgCAM

NgCAM-GFP was predominantly concentrated on axonal membranes, but its distribution within axons was uneven, highly concentrated in some branches and segments, but nearly invisible in others (Figs. 1A and 3E). We hypothesized that this pattern may result from the *trans* interactions between axons or the interaction with other binding proteins from contacting cells. To understand how NgCAM trafficking along axons may be affected by axonal bundling, we compared the movements of NgCAM-GFP in isolated and bundled axons using the FRAP imaging technique. In isolated axons, NgCAM-GFP-containing vesicles were mainly transported anterogradely (Fig. 7A left panel; movie 1). Interestingly, these transporting carriers often stopped at the crossing of NgCAM-GFP-containing axons (movie 1). In bundled axons, however, moving carriers were more difficult to visualize, partially due to their low fluorescence intensities (Fig. 7A right panel; movie 2).

To assess how different domains of NgCAM affect its axonal transport, we performed the FRAP imaging on three truncated mutants of NgCAM. Retrograde transport carriers of NgCAM-ΔCt significantly increased retrograde transport (Fig. 7B), compared to the wildtype. The axonal transport for NgCAM-ΔIg-GFP was still mainly in the anterograde direction (Fig. 7C). In contrast, the axonal transport of NgCAM-ΔFN-GFP significantly decreased in both directions (Fig. 7D). Furthermore, the average anterograde velocities of NgCAM-ΔFN-GFP (0.42 ± 0.05 μm/s; n = 43; One-way ANOVA, $F_{3, 174} = 9.231$, $P < 0.001$), NgCAM-ΔIg-GFP (0.49 ± 0.04 μm/s; n = 44; One-way ANOVA, $F_{3, 174} = 9.231$, $P = 0.002$) and NgCAM-ΔCt-GFP (0.42 ± 0.03 μm/s; n = 51; One-way ANOVA, $F_{3, 174} = 9.231$, $P < 0.001$) significantly decreased, compared to NgCAM-GFP (0.68 ± 0.04 μm/s; n = 43), while the average retrograde velocities (NgCAM-GFP: 0.37 ± 0.05 μm/s, n = 10, control; NgCAM-ΔFN-GFP: 0.32± 0.02 μm/s, n = 35, One-way ANOVA, $F_{3, 124} = 1.73$, $P = 0.557$; NgCAM-ΔIg-GFP: 0.41 ± 0.04 μm/s, n = 19, One-way ANOVA, $F_{3, 124} = 1.73$, $P = 0.824$; NgCAM-ΔCt-GFP: 0.33 ± 0.02 μm/s, n = 64, One-way ANOVA, $F_{3, 124} = 1.73$, $P = 0.630$) remained the same (Fig. 7E). Taken together, these data are consistent with the different targeting patterns of NgCAM deletion constructs.

Next, we examined how two axons move towards each other to form a bundle. Based on many works from both invertebrate and vertebrate systems, the current hypothesis is that the initial axons might play a pioneer-like role in establishing subsequent axonal tracts. The behaviors of growth cones are different for leading and following axons. This mode of axonal bundle formation was frequently observed in our system. For instance, the growth cone of a green axon touched and quickly elongated along the red axon (Fig. 7F; movie 3). The growth cone of green axon (the follower) was very small and did not display exploratory behavior (movie 3). Sometimes, new growth cones of the green axon were generated at the crossing and grew along the red axon (Fig. 7G; movie 4). Despite not being the primary focus of our studies, axon retraction, fragmentation (in pruning), and neuron cell death were also observed in our culture, which likely contribute to the de-bundling process of axons (Luo and O'Leary, 2005). Using our system, we also observed new lateral movements of bundling axons expressing NgCAM-GFP and NgCAM-mCherry. Following are the two representative movements that were observed in our culture. First, the two axonal fragments moved laterally towards each other, formed a contact in the middle, and then formed a bundle (Fig. 7H; movie 5). In this process, no filopodia-like structure was

observed. Second, two axons moved together in a zipper-like manner from one end to the other (Fig. 7I; movie 6). It is important to note that the lateral movements generally take place over a longer time, approximately 5-fold longer than that for guided axonal outgrowth. Once the moving axons contact with each other, the trans-homophilic interaction of NgCAM may stabilize the bundle, preventing bundled axons from debundling. Taken together, our studies suggest that the bundling of axonal networks most likely involves a combination of different movements of axons.

Discussion

In this study, we show that the polarized axon-dendrite targeting of expressed NgCAM regulates axonal and dendritic bundling of cultured hippocampal neurons. Axonal NgCAM specifically induced robust axonal bundling via the trans-homophilic interaction (Figs. 1,2). When the polarity of NgCAM targeting was reversed by either mutagenesis or kinase inhibitors, its expression induced dendritic bundling (Figs. 3–5). The effects of expressed NgCAM were applicable to mouse L1CAM (Fig. 6). Our time-lapse imaging studies further suggest that the trans-homophilic interaction of NgCAM may stabilize the bundle formation by regulating the intra-axonal transport and axonal movements (Fig. 7).

This *in vitro* study provides following mechanistic insights into biological functions of L1-CAM proteins in neural circuit formation. (1) Both proper homophilic interaction and axonal targeting are essential for L1-mediated axonal bundling or axon fasciculation. (2) Dendritic targeting of L1-CAM, at least transiently during development or induced by activity change, may regulate dendritic bundling or dendrite morphology. (3) Our study suggests activity dependent regulation of axon-dendrite targeting of L1-CAM via protein phosphorylation. The kinase cascade, the potential sorting signal within the FN domain, and how they affect L1-CAM axonal transport are interesting topics for future investigation. (4) The lateral movement of axons may be a major way for pre-targeting sorting in axonal bundling.

Our results suggest that different domains of L1-CAM are critical for ensuring its proper function in axonal bundling. The Ig domains that mediate the trans-homophilic interaction of NgCAM were required for axonal bundling in our system (Fig. 2), consistent with the notion that the Ig domains of L1-CAM mediate the cell-cell interaction (Kunz et al., 1998;Haspel and Grumet, 2003;Itoh et al., 2004;Maness and Schachner, 2007). Ig domains of L1 have additional binding partners involved in cell-cell interactions. Deleting the 6^{th} Ig domain of L1 prevented L1-L1 homophilic binding and L1 binding to RGD-dependent integrins, but did not disrupt interactions with neurocan or neuropilin (Itoh et al., 2004). Different from the L1 knockout mice (Cohen et al., 1998;Dahme et al., 1997;Fransen et al., 1997), knockin mice carrying the 6^{th} Ig deletion had normal corticospinal tract and corpus callosum, but developed severe hydrocephalus (Itoh et al., 2004). Deleting the intracellular C-terminal region of NgCAM moderately reduced axonal bundling (Fig. 2), suggesting that the C-terminus may play a regulatory role in the process. Although the C-terminal region contains major trafficking motifs and may initiate outside-in signaling in the cytosol, redundant routes may be available from the other membrane proteins that interact in *cis* with the extracellular domains of NgCAM. Our results are consistent with previous studies. Although L1 proteins maintain the homophilic adhesive activity in the absence of the cytoplasmic domain (Hortsch et al., 1995;Wong et al., 1995), mutations that reduce ankyrin binding reduce the homophilic adhesion of L1 proteins (Hortsch et al., 1998). A recent study further shows that the L1 cytoplasmic domain is dispensable for normal brain morphology, but is required for continued L1 protein expression and motor function in adult (Nakamura et al., 2010). Furthermore, our study show that the FN domain is required for axonal targeting of NgCAM (Fig. 4), consistent with a previous study (Sampo et al., 2003). Without this domain, NgCAM not only failed to effectively induce axonal bundling (Fig. 2D), but also

induced dendritic bundling. It is known that the FN domain of L1-CAM interacts with integrins and other CAMs (Haspel and Grumet, 2003;Maness and Schachner, 2007). How this domain regulates the axonal targeting of L1 and NgCAM remains to be determined in future studies.

Our data show that dendritic targeting of NgCAM and mL1CAM induced dendritic bundling (Figs. 3,6). Is it possible that L1-CAM proteins are involved in regulating dendritic bundling *in vivo*? Endogenous L1-CAM proteins do exist in dendrites at least transiently during development. Endogenous L1 co-localized with the dendritic marker MAP2 in cortical neurons at embryonic day 18 (Demyanenko et al., 1999). Moreover, the knockout mice with deleted CHL1 exhibited altered dendritic morphogenesis in cortical pyramidal neurons (Demyanenko et al., 2004). Furthermore, our data are consistent with previous studies that L1-CAM proteins regulate neurite outgrowth and fasciculation (Fischer et al., 1986;Martin et al., 2008;Yamamoto et al., 2006).

Endogenous L1 proteins in cultured hippocampal neurons do not inhibit the polarized axon-dendrite targeting of over-expressed NgCAM (Wisco et al., 2003; Sampo et al., 2003). The amount of over-expressed L1-GFP is approximately 5-fold higher than the endogenous L1 level (Dequidt et al., 2007). Endogenous L1 may contribute the background bundling in the late stage of hippocampal neurons in culture. This is consistent with our observation with mature hippocampal neurons (data not shown). In the relative early stage, due to the low expression level and interference from other axons, hippocampal neurons do not form stable axonal bundles. Although our study suggests the notion that the relative protein amount on axonal and dendritic membranes is crucial for proper neurite bundling can be applicable for both over-expressed and endogenous L1-CAM proteins, it requires caution that high protein levels of over-expression may result in non-physiological effects. Furthermore, we found that the effects of NgCAM on axonal and dendritic targeting/bundling were applicable to mouse L1CAM (Fig. 6). Since rat L1 is almost identical to mouse L1CAM, our study suggests that the expression level indeed are critical for the bundling. The relative protein levels on axonal and dendritic membranes are critical in polarized axon-dendrite targeting and hence in axonal and dendritic bundling. The stability of a neurite bundle may rely on the level of L1-CAM proteins. The expression of endogenous L1 proteins differs in different types of neurons and in different developmental stages, and may even be regulated by neuronal activity. Our study suggests that regulation of the L1 protein level may alter its polarized targeting, which in turn regulates axonal and dendritic bundling.

How is the polarized axon-dendrite targeting of L1-CAM regulated? Several putative axonal targeting motifs in NgCAM have been identified (Sampo et al., 2003; Wisco et al., 2003; Yap et al., 2008a). These motifs may conceivably act through their interacting proteins, such as other membrane proteins and cytoskeleton-associated proteins. Interestingly, L1-CAM binding to ankyrin B is regulated by the MAP kinase pathway (Whittard et al., 2006). Since the MAP kinase pathway is often activated by synaptic transmission, whether polarized targeting of L1-CAM can be regulated in an activity-dependent manner is an intriguing question for future research.

The activation of acetylcholine receptors by carbachol enhanced NgCAM-induced axonal bundling (Fig. 5A,E). Whereas changing neuronal excitability by blocking various Nav, Kv, and Cav channels did not significantly alter the axonal bundling, blocking protein kinase activities by the Stau treatment substantially decreased axonal bundling (Fig. 5E). The treatment also induced dendritic bundling (Fig. 5B), somewhat similar to the effect of expressing NgCAM-ΔFN-GFP (Fig. 3A–C). Interestingly, the Stau treatment reversed the polarity of axon-dendrite targeting of NgCAM-GFP (Fig. 5C). The effect of Stau may be partially mediated by a MAP kinase, JNK, since inhibiting JNK activity also significantly

reduced axonal bundling (Fig. 5E). Although other kinase blockers examined did not have significant effects, we cannot rule out the potential involvement of multiple protein kinases. Nonetheless, we have identified that two independent approaches, deleting the FN domain (Fig. 3) and the Stau treatment (Fig. 5), both reverse the polarity of L1-CAM axon-dendrite targeting and switch induced axonal to dendritic bundling. Our data have established the causal relationship between the polarized targeting of L1-CAM and proper neurite bundling.

How does the potential kinase pathway regulate the trafficking of L1-CAM proteins? We found that mobile carriers of NgCAM along bundled axons were much less abundant and with weaker intensity compared to isolated axons (Fig. 7A). This may be due to following reasons. First, NgCAM on the axonal membrane might transduce outside-in signaling into axons, inhibit the intra-axonal movement and hence recruit more NgCAM into the contact site. Second, since most NgCAM molecules were on axonal membranes and stabilized, much less NgCAM was available for movement within axons. Third, the trans-homophilic interaction of NgCAM on axonal membranes may initiate a signaling pathway to regulate axonal transport of NgCAM. These remain to be determined in future studies.

If axonal bundling exclusively results from the guided axonal outgrowth, merely as a consequence of axon guidance, we would not be able to explain how some of the patterns of axonal bundling formed in our culture. For instance, in NgCAM-induced axonal bundling, we often observed that axons formed bundles very close to the axon initial segments of the two neurons (Fig. 1A). Since we transfected neurons at 5 DIV when cultured hippocampal neurons already developed long processes of axons and dendrites, bundled axonal segments should not be close to the soma of both neurons. Cultured hippocampal neurons are a well-studied *in vitro* model and it is unlikely to generate an entire new axon after 5 DIV under normal conditions. Therefore, besides the mechanisms of guided axonal outgrowth, axon retraction, pruning, and cell death, other mechanism underlying axonal bundling must exist. Using our system, we indeed observed new lateral movements of bundling axons expressing NgCAM-GFP and NgCAM-mCherry. However, expressed NgCAM proteins may not be the driving force underlying the axon lateral movement, but their trans-homophilic interactions may stabilize the bundling process. The driving force of axonal lateral movement may be either intrinsic to the axonal shaft or mediated by a third cell, such as a contracting fibroblast, moving axonal growth cones from untransfected neurons, etc, which remains to be determined. The existence of axon lateral movement is supported by a recent study from the Jessell group (2006) suggesting that the sema6D/PlexinA1 pathway is involved in axonal shaft positioning of a group of sensory neurons projecting into the spinal cord, in which oligodendrocytes might mediate the movement (Yoshida et al., 2006). It is important to note that the mechanistic insights into axonal and dendritic bundling revealed by this *in vitro* study remain to be validated for physiological significance *in vivo*. Nonetheless, our studies open a new research avenue towards understanding the mechanisms and functions of axonal and dendritic bundling, which plays critical roles in the formation and remodeling of neural circuits.

Finally, the new assay system developed in this study offers unique advantages for mechanistic studies of neurite bundling. With this system, different constructs can be easily introduced in different neurons at different development stages, allowing for high-resolution and multi-color imaging analysis. Cultured hippocampal neurons develop sophisticated and well-characterized axons and dendrites, therefore highly suitable for studying neurite interactions. We also described a new parameter, ABI, to quantitatively reflect the degree of bundling. Furthermore, the combination of different timelapse imaging techniques to monitor axonal transport and axon movement advances our understanding of the dynamic nature of neurite bundling.

Supplementary Material

Refer to Web version on PubMed Central for supplementary material.

Acknowledgments

This work was supported by a Career Transition Fellowship Award from the National Multiple Sclerosis Society and a grant from National Institutes of Health to C.G.. We thank Drs. R. Tsien and G. Banker for sharing mCherry and NgCAM-GFP cDNAs, respectively, the University of Iowa Developmental Studies Hybridoma Bank (a non-profit facility) for mouse monoclonal anti-NgCAM 8D9 antibody, UC Davis/NIH NeuroMab facility (a non-profit facility) for mouse monoclonal anti-GFP antibody, Dr. R.J. Nelson for critical comments on the manuscript, Dr. W. Lai for assistance in statistical analysis, and Drs. S. Qin and M. Xu for technical assistance. All animal experiments have been conducted in accordance with the NIH Animal Use Guidelines.

The list of major abbreviations used in the paper

4-AP	4-aminopyridine
ABI	axonal bundling index
CHL1	close homolog of L1
DIV	day *in vitro*
FN	fibronectin
FRAP	fluorescence recovery after photobleaching
Ig	immunoglobulin
JNK	c-Jun N-terminal kinase
CAM	cell adhesion molecule
MAPK	mitogen-activated protein kinase
MAP2	microtubule associate protein 2
mCh	mCherry
Stau	staurosporine
TTX	tetrodotoxin

References

Bak M, Fraser SE. Axon fasciculation and differences in midline kinetics between pioneer and follower axons within commissural fascicles. Development. 2003; 130:4999–5008. [PubMed: 12952902]

Bastiani MJ, Raper JA, Goodman CS. Pathfinding by neuronal growth cones in grasshopper embryos. III. Selective affinity of the G growth cone for the P cells within the A/P fascicle. J Neurosci. 1984; 4:2311–2328. [PubMed: 6481449]

Bennett V, Chen L. Ankyrins and cellular targeting of diverse membrane proteins to physiological sites. Curr Opin Cell Biol. 2001; 13:61–67. [PubMed: 11163135]

Campbell RE, Gaidamaka G, Han SK, Herbison AE. Dendro-dendritic bundling and shared synapses between gonadotropin-releasing hormone neurons. Proc Natl Acad Sci U S A. 2009; 106:10835–10840. [PubMed: 19541658]

Cohen NR, Taylor JS, Scott LB, Guillery RW, Soriano P, Furley AJ. Errors in corticospinal axon guidance in mice lacking the neural cell adhesion molecule L1. Curr Biol. 1998; 8:26–33. [PubMed: 9427628]

Curtetti R, Garbossa D, Vercelli A. Development of dendritic bundles of pyramidal neurons in the rat visual cortex. Mech Ageing Dev. 2002; 123:473–479. [PubMed: 11796132]

Dahlin-Huppe K, Berglund EO, Ranscht B, Stallcup WB. Mutational analysis of the L1 neuronal cell adhesion molecule identifies membrane-proximal amino acids of the cytoplasmic domain that are required for cytoskeletal anchorage. Mol Cell Neurosci. 1997; 9:144–156. [PubMed: 9245498]

Dahme M, Bartsch U, Martini R, Anliker B, Schachner M, Mantei N. Disruption of the mouse L1 gene leads to malformations of the nervous system. Nat Genet. 1997; 17:346–349. [PubMed: 9354804]

De Angelis E, Watkins A, Schafer M, Brummendorf T, Kenwrick S. Disease-associated mutations in L1 CAM interfere with ligand interactions and cell-surface expression. Hum Mol Genet. 2002; 11:1–12. [PubMed: 11772994]

Demyanenko GP, Maness PF. The L1 cell adhesion molecule is essential for topographic mapping of retinal axons. J Neurosci. 2003; 23:530–538. [PubMed: 12533613]

Demyanenko GP, Tsai AY, Maness PF. Abnormalities in neuronal process extension, hippocampal development, and the ventricular system of L1 knockout mice. J Neurosci. 1999; 19:4907–4920. [PubMed: 10366625]

Demyanenko GP, Schachner M, Anton E, Schmid R, Feng G, Sanes J, Maness PF. Close homolog of L1 modulates area-specific neuronal positioning and dendrite orientation in the cerebral cortex. Neuron. 2004; 44:423–437. [PubMed: 15504324]

Dequidt C, Danglot L, Alberts P, Galli T, Choquet D, Thoumine O. Fast turnover of L1 adhesions in neuronal growth cones involving both surface diffusion and exo/endocytosis of L1 molecules. Mol Biol Cell. 2007; 18:3131–3143. [PubMed: 17538021]

Dickson TC, Mintz CD, Benson DL, Salton SR. Functional binding interaction identified between the axonal CAM L1 and members of the ERM family. J Cell Biol. 2002; 157:1105–1112. [PubMed: 12070130]

Escobar MI, Pimienta H, Caviness VS Jr, Jacobson M, Crandall JE, Kosik KS. Architecture of apical dendrites in the murine neocortex: dual apical dendritic systems. Neuroscience. 1986; 17:975–989. [PubMed: 3714046]

Fischer G, Kunemund V, Schachner M. Neurite outgrowth patterns in cerebellar microexplant cultures are affected by antibodies to the cell surface glycoprotein L1. J Neurosci. 1986; 6 :605–612. [PubMed: 3512794]

Fransen E, Van Camp G, Vits L, Willems PJ. L1-associated diseases: clinical geneticists divide, molecular geneticists unite. Hum Mol Genet. 1997; 6:1625–1632. [PubMed: 9300653]

Gu C, Zhou W, Puthenveedu MA, Xu M, Jan YN, Jan LY. The microtubule plus-end tracking protein EB1 is required for Kv1 voltage-gated K^+ channel axonal targeting. Neuron. 2006; 52:803–816. [PubMed: 17145502]

Hanson MG, Landmesser LT. Normal patterns of spontaneous activity are required for correct motor axon guidance and the expression of specific guidance molecules. Neuron. 2004; 43:687–701. [PubMed: 15339650]

Hanson MG, Landmesser LT. Increasing the frequency of spontaneous rhythmic activity disrupts pool-specific axon fasciculation and pathfinding of embryonic spinal motoneurons. J Neurosci. 2006; 26:12769–12780. [PubMed: 17151280]

Hanson MG, Milner LD, Landmesser LT. Spontaneous rhythmic activity in early chick spinal cord influences distinct motor axon pathfinding decisions. Brain Res Rev. 2008; 57:77–85. [PubMed: 17920131]

Haspel J, Grumet M. The L1CAM extracellular region: a multi-domain protein with modular and cooperative binding modes. Front Biosci. 2003; 8:s1210–1225. [PubMed: 12957823]

He S, Masland RH. ON direction-selective ganglion cells in the rabbit retina: dendritic morphology and pattern of fasciculation. Vis Neurosci. 1998; 15:369–375. [PubMed: 9605536]

Hortsch M, Wang YM, Marikar Y, Bieber AJ. The cytoplasmic domain of the Drosophila cell adhesion molecule neuroglian is not essential for its homophilic adhesive properties in S2 cells. J Biol Chem. 1995; 270:18809–18817. [PubMed: 7642532]

Hortsch M, Homer D, Malhotra JD, Chang S, Frankel J, Jefford G, Dubreuil RR. Structural requirements for outside-in and inside-out signaling by *Drosophila* neuroglian, a member of the L1 family of cell adhesion molecules. J Cell Biol. 1998; 142:251–261. [PubMed: 9660878]

Imai T, Yamazaki T, Kobayakawa R, Kobayakawa K, Abe T, Suzuki M, Sakano H. Pre-target axon sorting establishes the neural map topography. Science. 2009; 325:585–590. [PubMed: 19589963]

Itoh K, Cheng L, Kamei Y, Fushiki S, Kamiguchi H, Gutwein P, Stoeck A, Arnold B, Altevogt P, Lemmon V. Brain development in mice lacking L1-L1 homophilic adhesion. J Cell Biol. 2004; 165:145–154. [PubMed: 15067019]

Krieger P, Kuner T, Sakmann B. Synaptic connections between layer 5B pyramidal neurons in mouse somatosensory cortex are independent of apical dendrite bundling. J Neurosci. 2007; 27:11473–11482. [PubMed: 17959790]

Kunz S, Spirig M, Ginsburg C, Buchstaller A, Berger P, Lanz R, Rader C, Vogt L, Kunz B, Sonderegger P. Neurite fasciculation mediated by complexes of axonin-1 and Ng cell adhesion molecule. J Cell Biol. 1998; 143:1673–1690. [PubMed: 9852159]

Lin DM, Fetter RD, Kopczynski C, Grenningloh G, Goodman CS. Genetic analysis of Fasciclin II in Drosophila: defasciculation, refasciculation, and altered fasciculation. Neuron. 1994; 13:1055–1069. [PubMed: 7946345]

Lohmann C, Wong RO. Cell-type specific dendritic contacts between retinal ganglion cells during development. J Neurobiol. 2001; 48:150–162. [PubMed: 11438943]

Luo L, O'Leary DD. Axon retraction and degeneration in development and disease. Annu Rev Neurosci. 2005; 28:127–156. [PubMed: 16022592]

Maness PF, Schachner M. Neural recognition molecules of the immunoglobulin superfamily: signaling transducers of axon guidance and neuronal migration. Nat Neurosci. 2007; 10:19–26. [PubMed: 17189949]

Martin V, Mrkusich E, Steinel MC, Rice J, Merritt DJ, Whitington PM. The L1-type cell adhesion molecule Neuroglian is necessary for maintenance of sensory axon advance in the Drosophila embryo. Neural Dev. 2008; 3:10. [PubMed: 18397531]

Nakamura Y, Lee S, Haddox CL, Weaver EJ, Lemmon VP. Role of the cytoplasmic domain of the L1 cell adhesion molecule in brain development. J Comp Neurol. 2010; 518:1113–1132. [PubMed: 20127821]

Sampo B, Kaech S, Kunz S, Banker G. Two distinct mechanisms target membrane proteins to the axonal surface. Neuron. 2003; 37:611–624. [PubMed: 12597859]

Tosney KW, Landmesser LT. Development of the major pathways for neurite outgrowth in the chick hindlimb. Dev Biol. 1985; 109:193–214. [PubMed: 2985457]

Van Vactor D. Adhesion and signaling in axonal fasciculation. Curr Opin Neurobiol. 1998; 8:80–86. [PubMed: 9568395]

Walsh FS, Doherty P. Neural cell adhesion molecules of the immunoglobulin superfamily: role in axon growth and guidance. Annu Rev Cell Dev Biol. 1997; 13:425–456. [PubMed: 9442880]

Whittard JD, Sakurai T, Cassella MR, Gazdoiu M, Felsenfeld DP. MAP kinase pathway-dependent phosphorylation of the L1-CAM ankyrin binding site regulates neuronal growth. Mol Biol Cell. 2006; 17:2696–2706. [PubMed: 16597699]

Wiencken-Barger AE, Mavity-Hudson J, Bartsch U, Schachner M, Casagrande VA. The role of L1 in axon pathfinding and fasciculation. Cereb Cortex. 2004; 14:121–131. [PubMed: 14704209]

Wisco D, Anderson ED, Chang MC, Norden C, Boiko T, Folsch H, Winckler B. Uncovering multiple axonal targeting pathways in hippocampal neurons. J Cell Biol. 2003; 162:1317–1328. [PubMed: 14517209]

Wong EV, Cheng G, Payne HR, Lemmon V. The cytoplasmic domain of the cell adhesion molecule L1 is not required for homophilic adhesion. Neurosci Lett. 1995; 200:155–158. [PubMed: 9064600]

Xu M, Cao R, Xiao R, Zhu MX, Gu C. The axon-dendrite targeting of Kv3 (Shaw) channels is determined by a targeting motif that associates with the T1 domain and ankyrin G. J Neurosci. 2007; 27:14158–14170. [PubMed: 18094255]

Yamamoto M, Ueda R, Takahashi K, Saigo K, Uemura T. Control of axonal sprouting and dendrite branching by the Nrg-Ank complex at the neuron-glia interface. Curr Biol. 2006; 16:1678–1683. [PubMed: 16920632]

Yap CC, Lasiecka ZM, Caplan S, Winckler B. Alterations of EHD1/EHD4 protein levels interfere with L1/NgCAM endocytosis in neurons and disrupt axonal targeting. J Neurosci. 2010; 30:6646–6657. [PubMed: 20463227]

Yap CC, Nokes RL, Wisco D, Anderson E, Folsch H, Winckler B. Pathway selection to the axon depends on multiple targeting signals in NgCAM. J Cell Sci. 2008a; 121:1514–1525. [PubMed: 18411247]

Yap CC, Wisco D, Kujala P, Lasiecka ZM, Cannon JT, Chang MC, Hirling H, Klumperman J, Winckler B. The somatodendritic endosomal regulator NEEP21 facilitates axonal targeting of L1/NgCAM. J Cell Biol. 2008b; 180:827–842. [PubMed: 18299352]

Yoshida Y, Han B, Mendelsohn M, Jessell TM. PlexinA1 signaling directs the segregation of proprioceptive sensory axons in the developing spinal cord. Neuron. 2006; 52:775–788. [PubMed: 17145500]

Yu HH, Huang AS, Kolodkin AL. Semaphorin-1a acts in concert with the cell adhesion molecules fasciclin II and connectin to regulate axon fasciculation in Drosophila. Genetics. 2000; 156:723–731. [PubMed: 11014819]

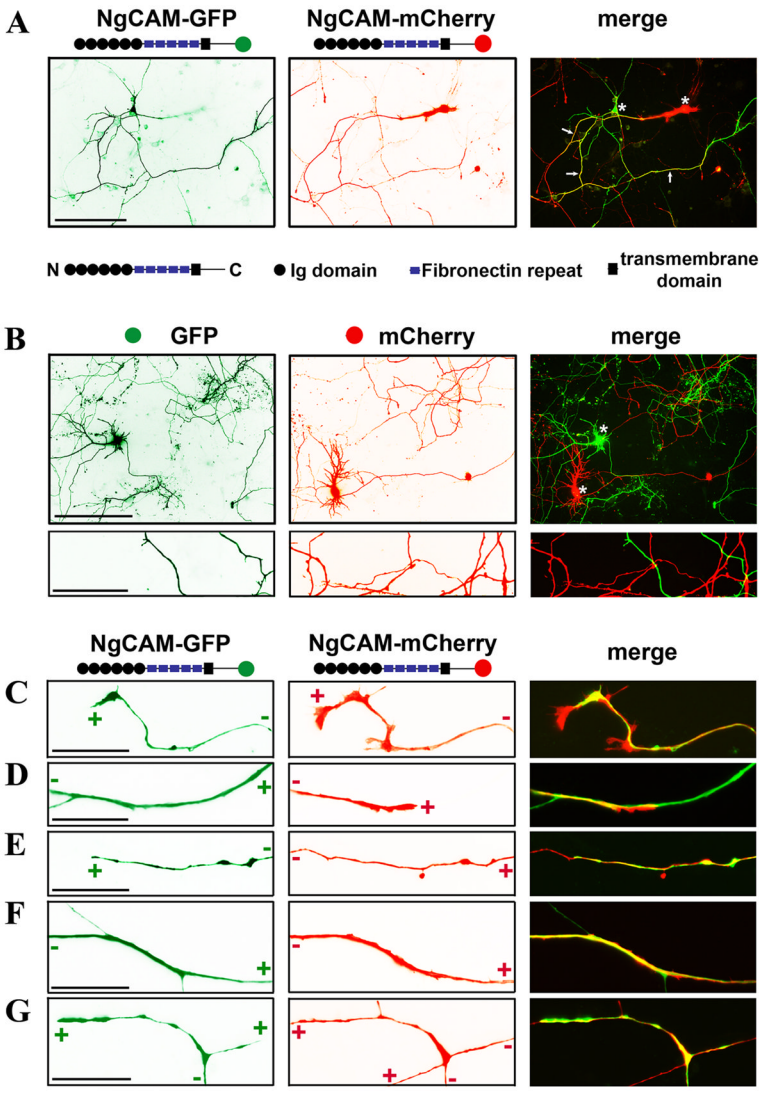

Fig. 1. Expression of NgCAM fusion proteins induced robust axonal bundling in cultured hippocampal neurons

Fluorescence proteins, GFP and mCherry, were fused to the C-terminus of NgCAM. Using a modified procedure, NgCAM-GFP and NgCAM-mCherry were transfected into different neurons in culture at 5 DIV and fixed 3 days later. (A) Extensive bundling was induced between the axons of NgCAM-GFP-and NgCAM-mCherry-expressing neurons. Structural diagrams of NgCAM constructs are provided. Black circles, the Ig domains; Purple rectangles, fibronectin repeats; The black squares, the membrane-spanning segment; Green and red circles, GFP and mCherry; “N” and “C”, the extracellular N- and intracellular C-terminus. Arrows, bundled axonal segments. (B) Despite many crossings, little bundling occurred between the axons of GFP- and mCherry-expressing neurons. The images in (C)-(G) in higher magnification show representative modes of axonal bundling in our culture. (C) Co-localization of two axonal growth cones expressing NgCAM-GFP and NgCAM-mCherry. (D) An axonal growth cone grew along a pioneer axon. (E) An axonal growth cone migrated in the reverse direction along an existing axon. (F) Bundled and isolated segments of a thin axon with a thick axonal bundle. (G) Branching of bundled axons. “+” and “−” indicate the directions of axonal growth cone and soma, respectively. Asterisks,

soma of transfected neurons. Scale bars, 100 μm in (A) and upper panels of (B), 10 μm in (C)-(G) and lower panels of (B).

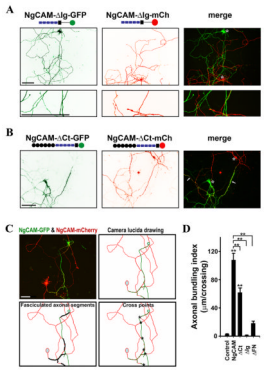

Fig. 2. Distinct roles of Ig and C-terminal domains of NgCAM in axonal bundling

(A) Deleting the Ig domains eliminated NgCAM-induced axonal bundling. Almost no axonal bundling was observed between NgCAM-ΔIg-GFP- and NgCAM-ΔIg-mCh-expressing neurons. NgCAM-ΔIg-GFP (green) and NgCAM-ΔIg-mCh (red) were transfected into different neurons at 5DIV and fixed three days later. (B) Deleting the intracellular C-terminal domain of NgCAM (NgCAM-ΔCt) moderately reduced axonal bundling. Axonal bundles were still abundantly present in culture. (C) Diagram for calculating the axonal bundling index (ABI). A pair of neurons expressing NgCAM-GFP (green) and NgCAM-mCherry (red) had bundled axonal segments. The camera lucida drawing is at the upper-right panel. Segments of axonal bundles are shown with thick black lines (lower left) and the crossings between green and red axons are indicated with asterisks (lower right). The ABI (104μm/crossing) of this pair of neurons equals to the total length of axonal bundles (624 μm) divided by the total number of crossings (6). (D) Summary of ABIs of NgCAM truncations. Control, between axons of GFP- and mCherry-expressing neurons; NgCAM, between axons of NgCAM-GFP- and NgCAM-mCherry-expressing neurons;ΔCt, between axons of NgCAM-ΔCt-GFP- and NgCAM-ΔCt-mCh-expressing neurons; ΔIg, between axons of NgCAM-ΔIg-GFP- and NgCAM-ΔIg-mCh-expressing neurons; ΔFN, between axons of NgCAM-ΔFN-GFP and NgCAM-ΔFN-mCh-expressing neurons. Asterisks, soma of transfected neurons. Scale bars, 100 μm. One-way ANOVA followed by Dunnett's test was used for the comparison to the control group; ** $P < 0.01$. Additional One-way ANOVA followed by Dunnett's test was performed for comparing the truncations to the wild type NgCAM shown on the top; ** $P < 0.01$.

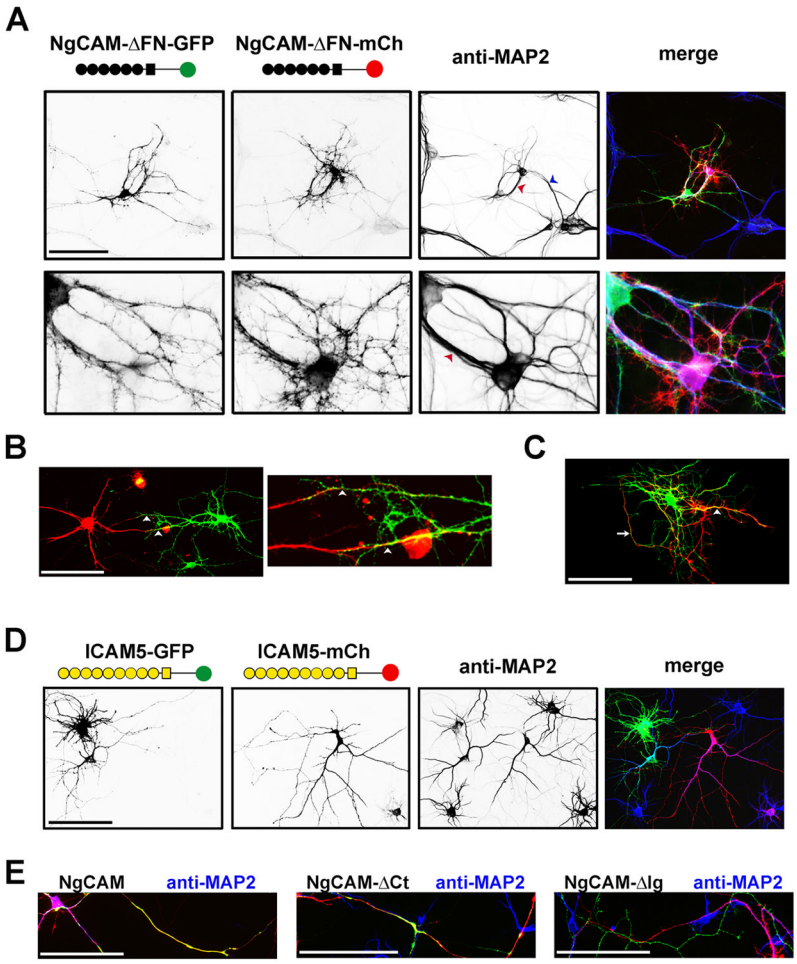

Fig. 3. Deleting the fibronectin repeats decreased axonal bundling but induced dendritic bundling

(A) The dendrites of a pair of neurons expressing NgCAM-ΔFN-GFP (green) and NgCAM-ΔFN-mCh (red) formed bundles in both parallel (blue arrowhead) and anti-parallel (red arrowhead) manners. The anti-MAP2 (microtubule associate protein 2) staining (blue in merged) indicated the dendrites and dendritic bundles. (B) Anti-parallel dendritic bundling. Dendrites of a pair of neurons expressing NgCAM-ΔFN-GFP (green) and NgCAM-ΔFN-mCh (red) grew towards each other and formed two bundles, indicated by white arrowheads. A high magnification image is provided on the right. (C) Parallel dendritic bundling. A pair of transfected neurons close to each other had an axonal bundle indicated by a white arrow and a parallel dendritic bundle indicated by a white arrowhead. (D) ICAM5 (telencephalin) constructs (ICAM5-GFP and ICAM5-mCh) were mainly localized in dendrites but did not induce dendritic bundling. Yellow circles, Ig domains; Yellow square, the membrane-spanning segment. (E) The axon-dendrite localization of NgCAM constructs revealed by dendritic marker MAP2. Neurons transfected with GFP (green) or mCherry (red) fused NgCAM constructs were stained with an anti-MAP2 antibody (blue). Scale bars, 100 μm.

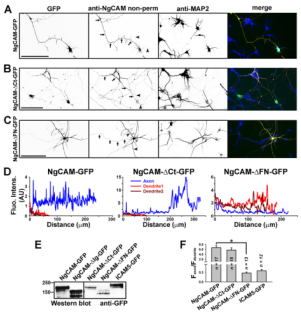

Fig. 4. Axon-dendrite targeting of NgCAM-GFP and its deletion mutants

Neurons transfected with NgCAM-GFP or its truncations were stained with anti-NgCAM antibody under non-permeabilized conditions, and then stained for MAP2, a dendritic marker, under permeabilized conditions. Signals are inverted in unmerged images. In merged images (right), GFP fluorescence is in green, anti-NgCAM staining in red, and anti-MAP2 staining in blue. (A) NgCAM-GFP was mainly localized on axonal membranes. (B) NgCAM-ΔCt-GFP was mainly localized on axonal membranes similar to the wildtype. (C) Deletion of the fibronectin repeat domain resulted in dendritic targeting of NgCAM-ΔFN-GFP. NgCAM-ΔFN-GFP was mainly enriched on dendritic membranes. Arrows, axons. Arrowheads, dendrites. Scale bars, 100 μm. (D) Surface levels of the three NgCAM constructs along the axon (blue) and two main dendrites (red and dark red). (E) Western blots of GFP fusion constructs expressed in HEK293 cells. Mouse monoclonal anti-GFP antibody was used. (F) Summary of polarized targeting of NgCAM and ICAM5 constructs. For NgCAM constructs the surface levels were measured, but for ICAM5-GFP the GFP fluorescence intensity reflecting the total protein level was measured. One-way ANOVA followed by Dunnett's test was used for the comparison among three NgCAM constructs; * $P < 0.001$.

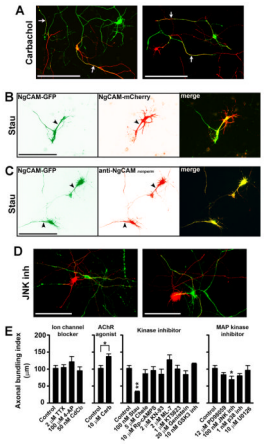

Fig. 5. Protein phosphorylation regulated axonal targeting of NgCAM and hence neurite bundling

Hippocampal neurons transfected with either NgCAM-GFP or NgCAM-mCherry at 5 DIV were incubated with various drugs for 2 to 3 days, and then fixed and stained for quantification of polarized targeting and axonal bundling. (A) The carbachol treatment enhanced axonal bundling. White arrows, bundled axons. (B) Inhibiting protein kinase activities by the Stau treatment markedly decreased axonal bundling but increased dendritic bundling. Black arrowheads, dendrites. (C) The Stau treatment resulted in dendritic targeting of NgCAM. (D) Inhibiting the JNK kinase activity significantly decreased axonal bundling. NgCAM-GFP in green and NgCAM-mCherry in red. Scale bars, 100 μm. (E) Summary of the effects of different drugs on NgCAM-induced axonal bundling. Four panels of drug treatment experiments included the effects of ion channel blockers, AChR agonist, kinase inhibitors, and MAP kinase inhibitors, from left to right. The same control group was used in the four panels. One-way ANOVA followed by Dunnett's test for comparing three or more groups, * $P < 0.05$. ** $P < 0.01$. Two-tailed Student's *t*-test for comparing two groups, * $P < 0.05$.

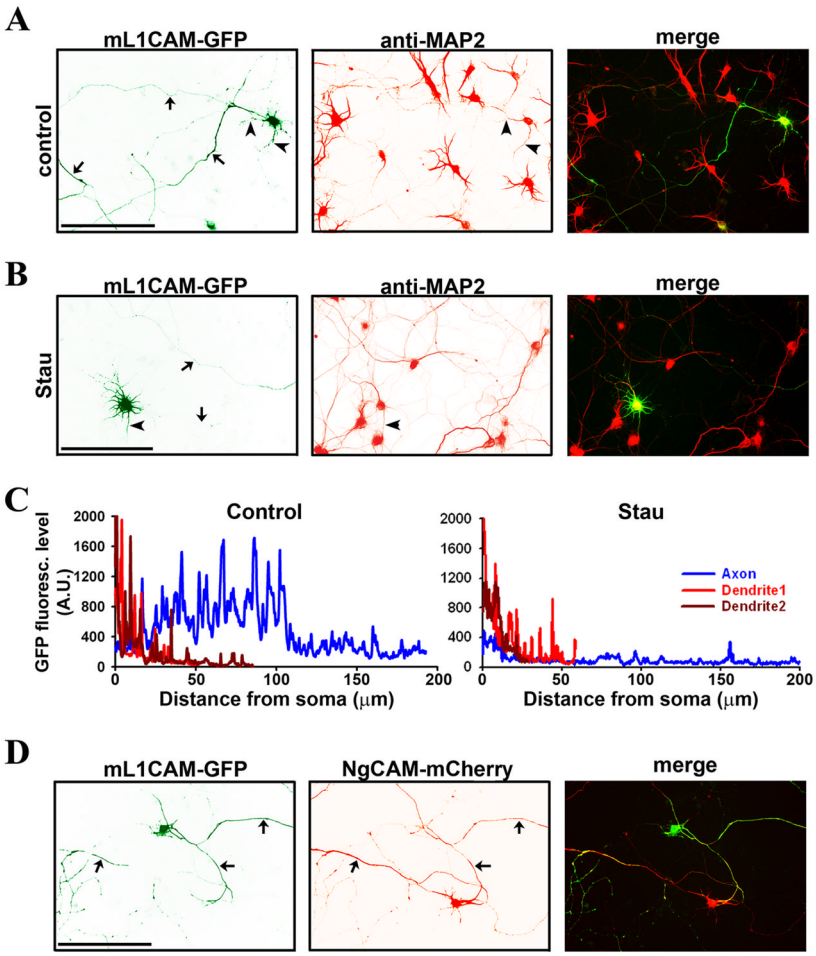

Fig. 6. Mouse L1-CAM (mL1CAM) axonal targeting is regulated by protein phosphorylation and induces axonal bundling

GFP was fused to the C-terminus of mL1CAM (mL1CAM-GFP). (A) When expressed in cultured hippocampal neurons, mL1CAM-GFP (green) mainly localized in axons. Dendrites were revealed with the MAP2 staining (red). (B) After treated with Stau, mL1CAM-GFP was mainly localized in dendrites but not axons. (C) GFP fluorescence levels of control (A) and Stau-treated neurons (B) along the axon (blue) and two main dendrites (red and dark red). Background value, 230, was subtracted. (D) mL1CAM-GFP-expressing axons formed bundles with NgCAM-mCherry-expressing axons. Arrows, axons. Arrowheads, dendrites. Scale bars, 100 μm.

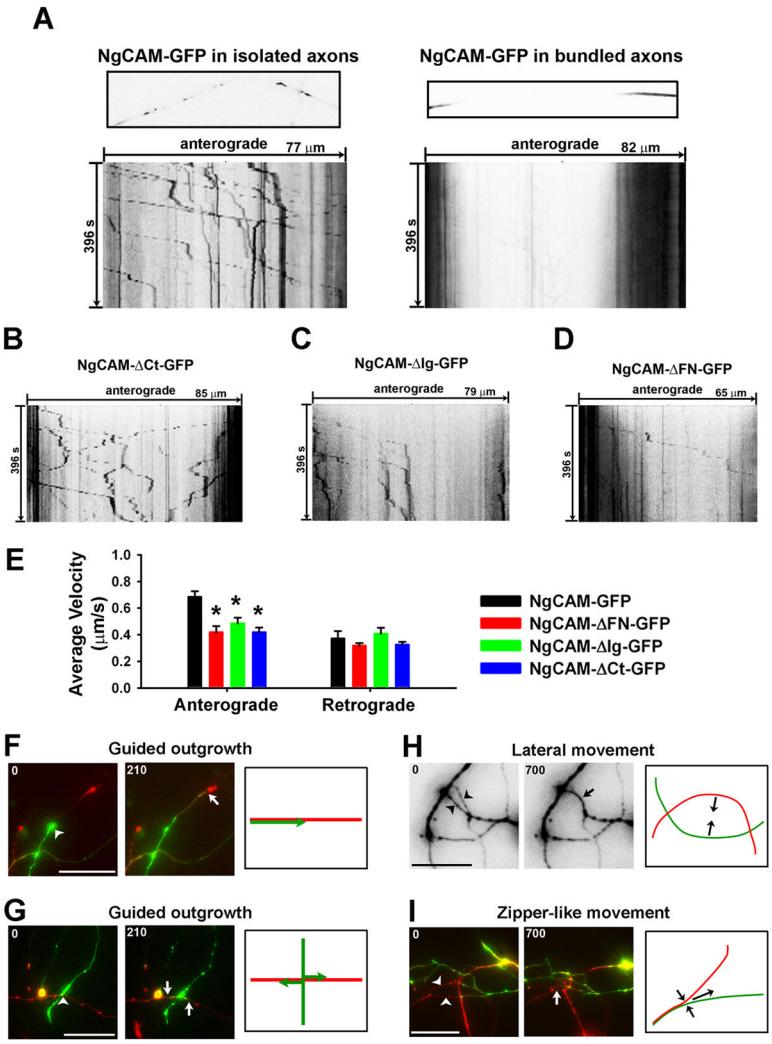

Fig. 7. Live cell imaging of NgCAM transport and neurite movements in bundle formation

(A) NgCAM-GFP-containing carriers moving anterogradely in an isolated axon (left) and reduced axonal transport in bundled axons (right). Many NgCAM-GFP molecules reflected by the strong GFP intensity were present in vesicular- and tubular-shaped carriers. The FRAP imaging experiments are shown by one frame of the axonal segment (upper) and the kymograph (lower). In kymographs, the total time (second) is indicated on the left, the total length (μm) on the top. (B) A kymograph of NgCAM-ΔCt-GFP axonal transport. (C) A kymograph of NgCAM-ΔIg-GFP axonal transport. (D) A kymograph of NgCAM-ΔFN-GFP axonal transport. (E) Reduced average velocity of anterograde but not retrograde axonal transport of the NgCAM mutations. One-way ANOVA followed by Dunnett's test. * $p < 0.05$. Long-term live-cell imaging revealed both guided axonal outgrowth ((F) and (G)) and lateral movements of axon shafts ((H) and (I)). (F) An axon (green) grew along a leading axon (red). (G) Two branches (green) were generated and grew along an existing axon (red) at a crossing. (H) Two axons moved towards each other laterally and formed a bundle. (I) Formation of a network of bundled axons included a zipper-like movement and guided axon outgrowth. Arrowheads indicate another kind of lateral movement, zipper-like movement. The first and last frames are provided, and the model diagram drawing is on the right. Arrowheads, beginning positions; Arrows, ending positions. Numbers at the upper-left corner, time in minutes. Scale bars, 20 μm.